STUDY AND REGULATION OF DC BUS VOLTAGES OF WIND-PHOTOVOLTAIC SYSTEM

SALIHA AREZKI [1], MOHAMED BOUDOUR [2]

Key words: Wind system, Photovoltaic (PV) system, Maximum power point tracking (MPPT), Doubly fed induction generator (DFIG), Fuzzy logic control.

In this paper, we study the unbalance problem of the input Direct Current (DC) voltages of the five-level neutral point clamping (NPC) voltage source inverter (VSI) used in hybrid renewable energy system. The hybrid system is composed of doubly fFed induction generator (DFIG) driven by wind turbine, the rotor is connected to three five-level NPC VSI feed by photovoltaic voltage source. We show particularly the problem of the instability of the DC voltages of the inverter and its consequence on the performances of the DFIG. Then, we propose a solution by using fuzzy logic technique in closed loop regulation. We add clamping bridge to stabilize the four DC input voltages of the five-level NPC. The results are full of promise to be used to stabilize the input DC voltages of the five-level NPC VSI in this kind of application.

1. **INTRODUCTION**

In the last decade, the wind energy maintains a growth of 30 % per year [1, 2]. In Algeria, the wind reaches intensities around 6 to 7 m/s in the regions of the South-West, this speed is enough to power generation of high power that can be used for domestic consumption. Moreover Algeria has bigger solar radiation, specifying that the average duration of period of sunshine exceeds the annual 2 600 hours to reach nearly 3 500 hours of sunshine in the dessert of Sahara.

Hybrid system which consists of wind energy and solar photovoltaic (PV) is realized to obtain a parallel functioning of these two sources, and to ensure the training of the DFIG and to generate maximum power with best efficiency [1, 2].

In this paper, we aim to solve the problem of instability caused by the fluctuations at the input voltages resulting of using multilevel inverter with five-level NPC structure. We propose the use of feedback loop to regulate the total average DC voltages of the inverter by using fuzzy logic control (FLC) and equalizing the DC capacitor voltages in all the levels by using a clamping bridge.

[1] Laboratory of Electrical & Industrial Systems, BP.32 El-Alia, Bab Ezzouar 16111 Algiers, Algeria, E-mail: arezki.saliha@gmail.com

[2] E-mail: mboudour@ieee.org

Rev. Roum. Sci. Techn. – Électrotechn. et Énerg., **59**, *1,* p. 35–46, Bucarest, 2014

2. PRESENTATION OF HYBRID PHOTOVOLTAIC-WIND SYSTEM

The schematic presentation in its simplest form of the hybrid energy conversion system proposed is given in Fig. 1. This system consists of following elements: a doubly fed induction generator (DFIG), a wind turbine, a photovoltaic generator and an inverter of five-level NPC VSI.

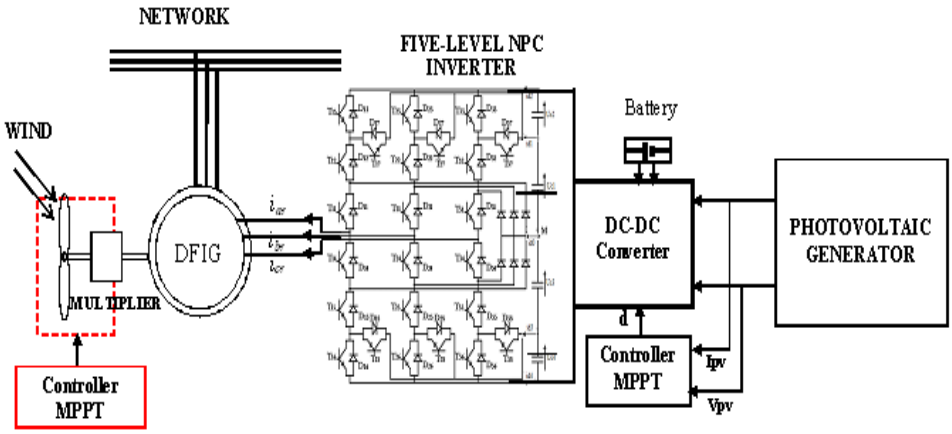

Fig. 1 – Schematic illustration of the hybrid chain energy conversion.

The wind turbine converts the kinetic energy of wind into mechanical energy, which is transformed in electrical form by the DFIG and transmitted to the network. The rotor of the DFIG is connected to an inverter of five-level NPC VSI ; the inverter is fed by the whole photovoltaic generator (PVG) and DC-DC converter. The choice of the multilevel converter is to synthesize a sinusoidal form of the voltage with less harmonic distortion. However, it presents a fluctuating potential of mid-point inducing instability of its input voltages, and then instability of its output voltages. Different PWM algorithms of the five-level NPC VSI are possible, the best one is the vector modulation strategy with four bipolar carriers [3, 4].

3. MODELING OF THE HYBRID SYSTEM

3.1. MODELING OF THE AEROTURBINE

The aeroturbine is composed of three pales of length R on one tree, a turbine and a gearbox with a gain G [1, 2, 5]. The generator shaft is modeled by the following equation:

$$J\frac{\mathrm{d}}{\mathrm{d}t}\Omega_{\mathrm{mec}} = C_{\mathrm{g}} - C_{\mathrm{em}} - f\,\Omega_{\mathrm{mec}}\,, \tag{1}$$

$$C_{\mathrm{g}} = \frac{C_{\mathrm{aer}}}{G}, \quad C_{\mathrm{air}} = \frac{P_{\mathrm{aer}}}{\Omega_{\mathrm{tur}}}, \quad \Omega_{\mathrm{mec}} = G \quad \Omega_{\mathrm{tur}} \quad , \tag{2}$$

where: J is the total inertia of rotating parts (kg·m^2); f – the viscous friction coefficient ; C_{em} – the electromagnetic torque of the generator (N·m); C_{g} is the mechanical torque in the output of multiplier; C_{aer} is the aerodynamic torque of the turbine; G – the gain of the multiplier; Ω_{mec} – generator speed; Ω_{tur} – turbine speed. The aerodynamic power recovered at the rotor of the turbine P_{aer} is:

$$P_{\mathrm{aer}} = C_{\mathrm{p}}(\lambda, \ \beta) \ \frac{\rho}{2} \ v^3 s \, . \tag{3}$$

The power coefficient C_{p}, is the aerodynamic efficiency of the turbine. Its theoretical limit is given by the Betz limit. In our case the power coefficient C_{p} and the speed ratio λ are defined by the following equation [2]:

$$\lambda = \frac{\Omega_{\mathrm{tur}} \quad R}{v}, \tag{4}$$

$$C_{\mathrm{p}}(\lambda, \ \beta) = \frac{\rho}{2} C_1 \left(\frac{C_2}{\lambda_i} - C_3 \beta - C_4 \right) \ \mathrm{e}^{-\frac{C_5}{\lambda_i}} + C_6 \lambda \, , \tag{5}$$

in which: $\lambda_i = \dfrac{1}{\lambda + 0.008\,\beta} - \dfrac{0.035}{\beta^3 + 1}$, where: $C_1 = 0{,}5176$, $C_2 = 116$, $C_3 = 0.4$, $C_4 = 5$, $C_5 = 21$, $C_6 = 0.0068$, and ß is the pitch angle, v is the wind speed.

3.2. MODELING OF THE DFIG

The modeling of the DFIG in the frame of Park is given as follow [2, 5]:

$$\begin{cases} V_{\mathrm{ds}} = R_{\mathrm{s}} \quad i_{\mathrm{ds}} + \dfrac{\mathrm{d}}{\mathrm{d}t}\varphi_{\mathrm{ds}} - \omega_{\mathrm{s}}\varphi_{\mathrm{qs}} \\ V_{\mathrm{qs}} = R_{\mathrm{s}} \quad i_{\mathrm{qs}} + \dfrac{\mathrm{d}}{\mathrm{d}t}\varphi_{\mathrm{qs}} + \omega_{\mathrm{s}}\varphi_{\mathrm{ds}} \end{cases} \quad \begin{cases} V_{\mathrm{dr}} = R_{\mathrm{r}} \, i_{\mathrm{dr}} + \dfrac{\mathrm{d}}{\mathrm{d}t}\varphi_{\mathrm{dr}} - (\omega_{\mathrm{s}} - \omega_{\mathrm{r}})\varphi_{\mathrm{qr}} \\ V_{\mathrm{qr}} = R_{\mathrm{r}} \, i_{\mathrm{qr}} + \dfrac{\mathrm{d}}{\mathrm{d}t}\varphi_{\mathrm{qr}} + (\omega_{\mathrm{s}} - \omega_{\mathrm{r}})\varphi_{\mathrm{dr}} \end{cases} . \tag{6}$$

Flux-currents relations are given by:

$$\begin{cases} \varphi_{\mathrm{ds}} = L_{\mathrm{s}} i_{\mathrm{ds}} + M \, i_{\mathrm{dr}} \\ \varphi_{\mathrm{qs}} = L_{\mathrm{s}} i_{\mathrm{qs}} + M \, i_{\mathrm{qr}} \end{cases} \quad \begin{cases} \varphi_{\mathrm{dr}} = L_{\mathrm{r}} i_{\mathrm{dr}} + M \, i_{\mathrm{ds}} \\ \varphi_{\mathrm{qr}} = L_{\mathrm{r}} i_{\mathrm{qr}} + M \, i_{\mathrm{qs}} \end{cases} , \tag{7}$$

$$C_{em} = p\frac{M}{L_s}\left(\varphi_{qs}\ \ i_{dr} - \varphi_{ds}\ \ i_{qr}\right), \tag{8}$$

where: R_s is stator resistance, R_r – rotor resistance, L_s is stator inductance, M – mutual inductance, φ_{ds}, φ_{qs} are respectively direct and quadrature stator flux, φ_{dr}, φ_{qr} are respectively direct and quadrature rotor flux, i_{ds}, i_{qs} are respectively direct and quadrature stator current, i_{dr}, i_{qr} are respectively direct and quadrature rotor current, p – number of pair poles, ω_r, ω_s – angular speed respectively of rotor and of stator.

3.3. MODEL OF SOLAR PHOTOVOLTAIC

Several models of photovoltaic cells exist [3, 6, 7, 8]. In this paper, we chose the model of two exponential as shown in Fig. 2 [3, 7].

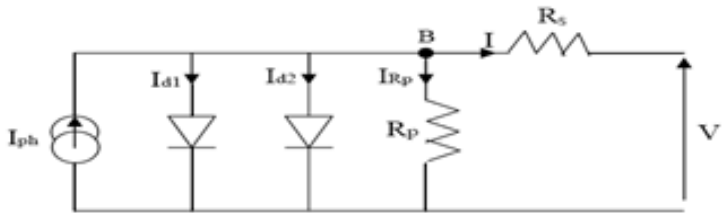

Fig. 2 – Model of a two-exponential solar cell.

The characteristic equations of a photovoltaic panel consisting of N_s cells connected in series are given as follow [3, 7]:

$$I = I_{ph}\big|_{T=298}\cdot\left[1+(T-289)5\cdot10^{-4}\right] - I_{S1}\left[e^{\frac{q(V+R_sI)}{A_1KT}}-1\right] - I_{S2}\left[e^{\frac{q(V+R_sI)}{A_2KT}}-1\right] - \frac{V+R_sI}{R_p}, \tag{9}$$

with : $I_{ph}\big|_{T=298} = 3.25\ \text{A}$, $I_{S1} = K_1T^3e^{-\frac{E_g}{KT}}$, $K_1 = 1.2\ \text{A/Cm}^2\text{K}^3$, $I_{S2} = K_2T^{\frac{5}{2}}e^{-\frac{E_g}{KT}}$, $K_2 = 2.9\cdot10^{\frac{5}{2}}\ \text{A/Cm}^2\text{K}^3$, where : I and V are current and output voltage of the photovoltaic cell; I_{ph} is the photo-current product; I_{S1} and I_{S2} are the saturation currents of diodes; A_1 and A_2 are the factors of purity of the diode (A_1 = 1 and A_2= 2); R_S and R_P are respectively the series resistance and parallel resistance; T is the absolute temperature in Kelvin; q – the elementary charge constant; K – the Boltzmann constant; E_g – the energy band of semi-conductor.

3.4. MODEL OF DC BUS

Fig. 3 shows the structure of the DC bus [9]. The model of this DC bus is defined as follow:

$$\begin{cases} C_1 \dfrac{\mathrm{d}U_{c1}}{\mathrm{d}t} = I_{\mathrm{pv}} - i_{\mathrm{d}_2} - i_{\mathrm{d}_1} \\ C_3 \dfrac{\mathrm{d}U_{c3}}{\mathrm{d}t} = I_{\mathrm{pv}} + i_{\mathrm{d}_3} + i_{\mathrm{d}_4} \end{cases} \quad \begin{cases} C_2 \dfrac{\mathrm{d}U_{c2}}{\mathrm{d}t} = I_{\mathrm{pv}} - i_{\mathrm{d}_2} \\ C_4 \dfrac{\mathrm{d}U_{c4}}{\mathrm{d}t} = I_{\mathrm{pv}} + i_{\mathrm{d}_4} \end{cases}. \tag{10}$$

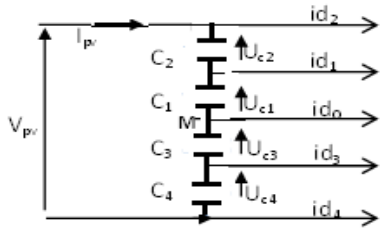

Fig. 3 – Structure of the DC voltages bus.

4. **POWER CONTROL OF THE DFIG**

In Park model, the active and reactive powers of DFIG are written [1]:

$$\begin{cases} P = V_{\mathrm{ds}}\, i_{\mathrm{ds}} + V_{\mathrm{qs}}\, i_{\mathrm{qs}} \\ Q = V_{\mathrm{qs}}\, i_{\mathrm{ds}} - V_{\mathrm{ds}}\, i_{\mathrm{qs}} \end{cases}. \tag{11}$$

By orienting the stator flux on d-axis: $\phi_{ds}= \phi$, $\phi_{qs}=0$ [1, 5], which makes the electromagnetic torque and consequently the active power, only dependent on i_{qr}, for the machines of large power, the resistance of the winding statoric R_{s} being neglected. From equation (6–8, 11) we can obtain [1, 2, 5]:

$$\begin{cases} P_{\mathrm{s}} = -V_{\mathrm{s}} \dfrac{M}{L_{\mathrm{s}}} i_{\mathrm{qr}} \\ Q_{\mathrm{s}} = \dfrac{V_{\mathrm{s}}\, \Phi_{\mathrm{s}}}{L_{\mathrm{s}}} - \dfrac{V_{\mathrm{s}}\, M}{L_{\mathrm{s}}} i_{\mathrm{dr}} \end{cases}. \tag{12}$$

From (6–8), the rotor voltage can be rewritten[1, 2, 5]:

$$\begin{cases} V_{\mathrm{dr}} = R_{\mathrm{r}}\, i_{\mathrm{dr}} + \left(L_{\mathrm{r}} - \dfrac{M^2}{L_{\mathrm{s}}} \right) \dfrac{\mathrm{d}}{\mathrm{d}t} i_{\mathrm{dr}} - g\omega_{\mathrm{s}} \left(L_{\mathrm{r}} - \dfrac{M^2}{L_{\mathrm{s}}} \right) i_{\mathrm{qr}} \\ V_{\mathrm{qr}} = R_{\mathrm{r}}\, i_{\mathrm{qr}} + \left(L_{\mathrm{r}} - \dfrac{M^2}{L_{\mathrm{s}}} \right) \dfrac{\mathrm{d}}{\mathrm{d}t} i_{\mathrm{qr}} - g\omega_{\mathrm{s}} \left(L_{\mathrm{r}} - \dfrac{M^2}{L_{\mathrm{s}}} \right) i_{\mathrm{dr}} + g \dfrac{MV_{\mathrm{s}}}{L_{\mathrm{s}}} \end{cases}. \tag{13}$$

It is possible to describe the control of this system by Fig.4 [1].

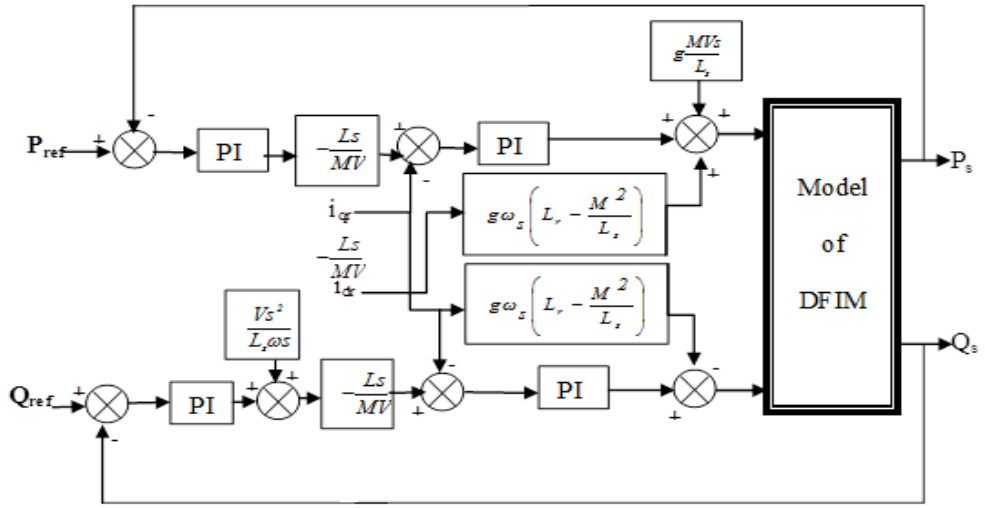

Fig. 4 – Block scheme of the structure of indirect control by stator flux orientation.

6. **PROBLEM OF FLUCTUATION IN DC BUS**

Several works [9, 10] raised problems of fluctuation at the input voltages of the inverter of five-level NPC structure inducing instability of the voltages supplied. The unbalance of the different DC voltages sources of the five-level NPC VSI constituted the major limitation for the use of this power converter [9].

We propose solutions which use feedback control by a regulation in closed loop control using fuzzy logic regulation. The clamping bridge is added to improve the regulation.

6.1. **FUZZY LOGIC METHOD**

6.1.1. PRINCIPLE

The principle of fuzzy control is based on the following three blocks: Fuzzification of input variables which are defined by linguistic variables (fuzzy sets or subsets), then the Inference where these variables are compared with predefined sets to determine appropriate response. And finally Defuzzification, to convert the subset fuzzification in values, using the centroid defuzzification. The basic structure of our fuzzy controller is shown in Fig. 5 [3, 11, 12].

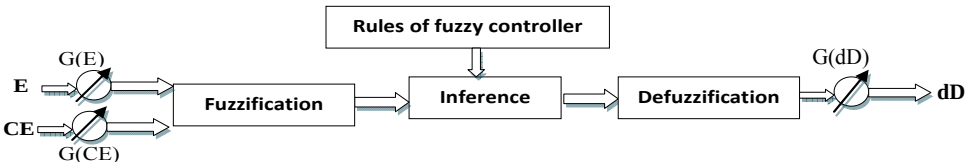

Fig. 5 – Basic structure of fuzzy controller.

The error E and change of error CE, at sampling instants k, are defined as follows:

$$E(k) = \frac{P_{Pv}(k) - P_{Pv}(k-1)}{V_{Pv}(k) - V_{Pv}(k-1)} \quad , \quad CE(k) = E(k) - E(k-1) \, , \tag{14}$$

$P_{pv}(k)$ and $V_{pv}(k)$ are respectively the power and voltage of PVG. The $G(E)$, $G(CE)$, $G(dd)$ are adaptation gain of our controller.

The input $E(k)$ shows if the load operation point at the instant k is located on the left or on the right of the maximum power point on the PV characteristic, while the input $CE(k)$ expresses the moving direction of this point. The fuzzy inference is carried out by using Mamdani method. The defuzzification uses the centre of gravity to compute the output of the fuzzy logic controller which is the duty cycle:

$$D = \frac{\sum_{j=1}^{n} \mu(D_J) - D_j}{\sum_{j=1}^{n} \mu(D_j)} \tag{15}$$

where – ($\mu(D_j)$ membership function of duty cycle D for point j ; D_j – duty cycle D for point j).

Table 1 shows one of possible control rules base. The rows represent the error change CE and the columns represent the rate of the error E. Each pair (E, CE) determines the output level corresponding to D,

Table 1

Rules base of fuzzy logic controller

CE / *E*	*NB*	*NS*	*ZE*	*PS*	*PB*
NB	*ZE*	*ZE*	*PB*	*PB*	*PB*
NS	*ZE*	*ZE*	*PS*	*PS*	*PS*
ZE	*PS*	*ZE*	*ZE*	*ZE*	*NS*
PS	*NS*	*NS*	*NS*	*ZE*	*ZE*
PB	*NB*	*NB*	*NB*	*ZE*	*ZE*

where: *NB* is negative big, *NS* – negative small, *ZE* – zero, *PS* – positive small and *PB* – positive big. These acronyms are labels of fuzzy sets and their corresponding membership functions are depicted in Fig. 6 [3].

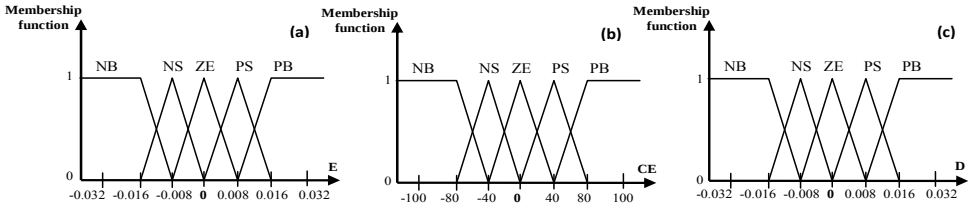

Fig. 6 – Membership functions of: (a) error *E*; (b) change of error *CE*; (c) duty ratio *D*.

6.1.2. FEEDBACK CONTROL OF FIVE-LEVEL NPC INVERTER

To alleviate the problem of the instability of the input DC voltages in the five-level NPC inverter, we propose to use a fuzzy logic regulator. The principle of this controller is the same as developed before, where error *E* and change of error *CE* are the inputs and I_{cref} is the output

$$\begin{cases} E = U_{ref} - U_{cmoy} \\ CE = E(k) - E(k-1) \end{cases} \qquad U_{Cmoy} = \frac{Uc_1 + Uc_2 + Uc_3 + Uc_4}{4}, \tag{16}$$

where U_{ref} – reference voltage corresponding to the average input voltage of the inverter; U_{cmoy}: average input voltage of the inverter; *E* – error of the two voltages (reference average voltage and the average voltage); *CE* – variation of the error *E* between the moment *k* and the moment *k* – 1.The general principle enslavement of five-level inverter is given by Fig. 7.

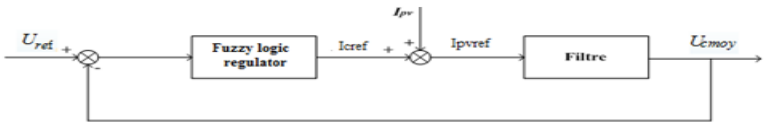

Fig. 7 – Enslavement algorithm of output voltage of five-level inverter.

6.2. INTRODUCTION OF CLAMPING BRIDGE CIRCUIT

This circuit is composed of transistor and a resistor placed in series across each capacity of the DC bus, Fig. 8 [9, 10].

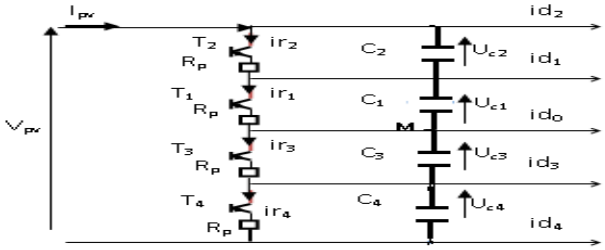

Fig. 8 – Structure of the capacitif filter with clamping bridge.

The control algorithm of the clamping bridge is given by [10]:

$$i_{\mathrm{ri}} = \frac{U_{\mathrm{ci}}}{R_{\mathrm{p}}} T_i \quad \text{if} \quad U_{\mathrm{ci}} \geq 200 \quad \text{else} \quad 0 \quad (i=1\div 4). \tag{17}$$

7. SIMULATION RESULTS

The wind profile used in our model is shown in Fig. 9. The application of this profile in our system shows that the variation of the mechanical speed of the generator, which turns at 157 rad/ s, or around 1 500 rpm.

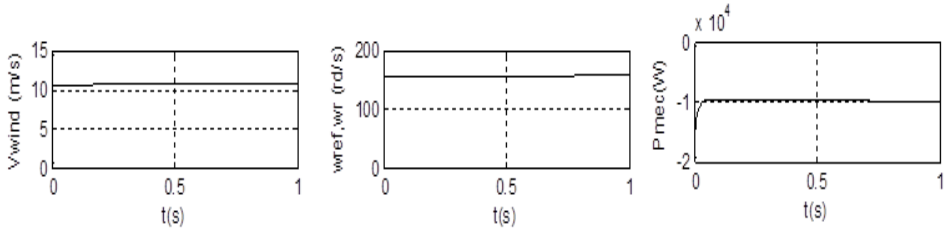

Fig. 9 – Wind profile model applied with mechanical speed of the generator.

Figure 10 shows perfectly the problem of the unbalance of the four voltages of the DC bus. Voltages are increasing.

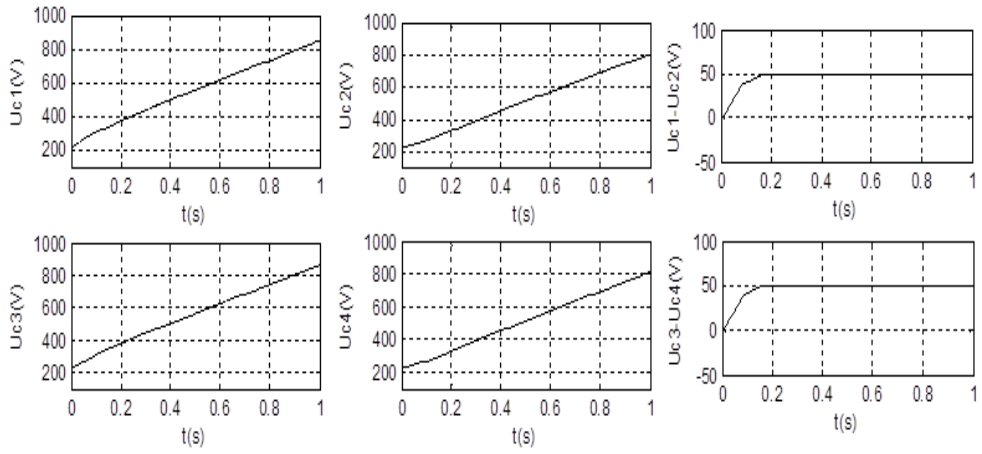

Fig. 10 – The DC bus voltages and their differences without clamping bridge.

By using the clamping bridge as a technique of stabilisation, we notice from Fig. 11, that the input voltages of the five-level NPC VSI stabilise around 220V.

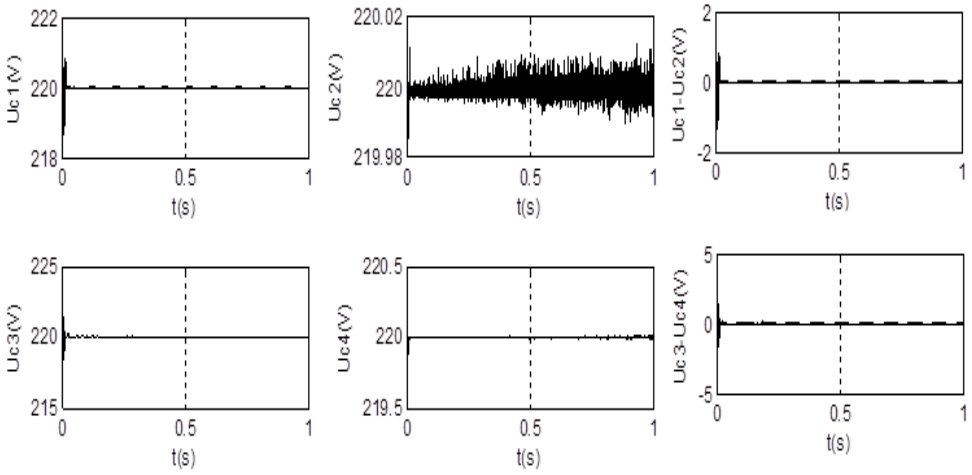

Fig. 11 – The DC bus voltages and their differences
with clamping bridge.

Figure 12a shows important undulations of the current, torque (undulations due to the instability of the rotor voltages) and Fig. 12b shows that the undulations on the performances (torque and current) disappear after introduction of the clamping bridge.

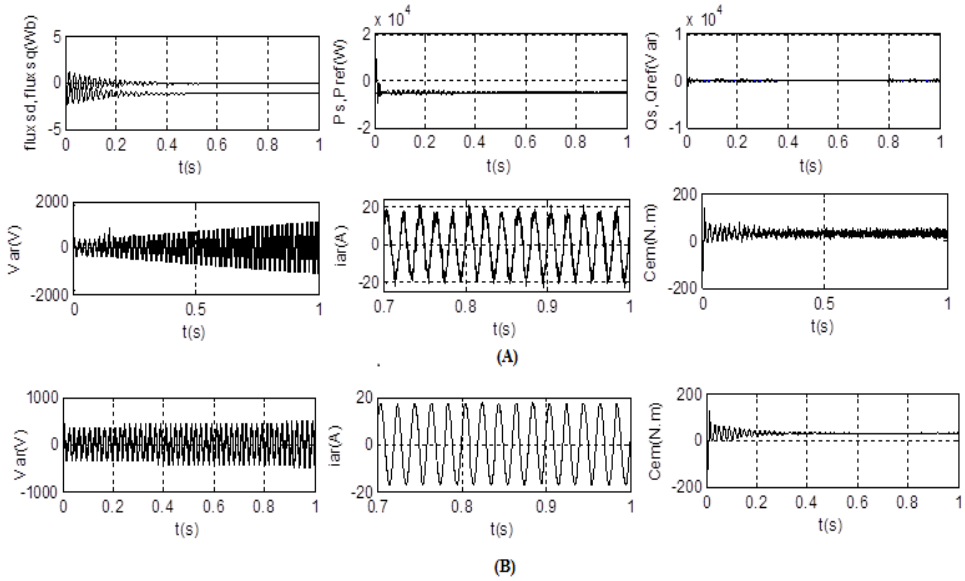

Fig. 12 – The performances of DFIG: A) without clamping bridge;
B) with clamping bridge.

8. **CONCLUSION**

In this paper, we have shown the effect of the instability of the DC voltages on the performances of the DFIG using in wind-photovoltaic system. The use of multilevel inverter system has two roles: form a sinusoidal shape and minimize the amount of harmonic distortion. The simulation results have shown the instability of the rotor voltages due to the instability of input voltages of the multilevel converter. The regulation of these voltages is provided by the fuzzy logic technique. The application of the fuzzy logic regulation has stabilized the input average voltage of the inverter but not each input voltages. The addition of Clamping Bridge gives the perfect stabilization of the input voltages of the five-level NPC VSI. These solutions improve the overall performances of the DFIG.

APPENDIX

DFIG: P = 7.5 kW; 220/380V– 50 Hz ; 15/8.6 A ; 1450 rpm ; J = 0.3126 kg·m^2 ; f = 0.00673 N·m·s/rad; P = 2 ; R_s =1.2 Ω ; R_r = 1.8 Ω ; L_s = 0.1554 H ; L_r = 0.1568 H; P_{ref} = –5000 W, Q_{ref} = 0 var, Cr = – 49Nm.

Turbine: R = 3 m ; G = 5.4 ; J = 0.0017 kg ·m^2 ; f = 0.0024 Nms/rad.

Filter: C_1= C_2 = C_3 = C_4= 20 mF ; U_{ref} = U_{cref} = 200 V ; R_p = 10 Ω ; f_p = 2 kHz.

Received on February 15, 2013

REFERENCES

1. S. El Aimani*, Modélisation de différentes technologies d'éoliennes intégrées dans un réseau de moyenne tension,* Ecole Centrale de Lille, Université des Sciences et Technologies de Lille, 2004.
2. F. Poitiers, *Etude et commande de génératrices asynchrones pour l'utilisation de l'énergie éolienne, machine asynchrone à cage autonome, machine asynchrone à double alimentation reliée au résea,* Université de Nantes, 2003.
3. M. Hatti, *Contrôleur flou pour la poursuite du point de puissance maximum d'un système photovoltaïque,* JCG'08 Lyon, 16 et 17 Décembre 2008.
4. A. G. Aissaoui, *A. Tahour*, *Application of Fuzzy Logic in Control of Electrical Machines*, in book: *Fuzzy Logic – Controls*, *Concepts*, *Theories and Applications*, Edited by Elmer P. Dadios. (ISBN 978-953-51-0396-7). First published March, 2012, by InTech Janeza Trdine 9, 51000 Rijeka, Croatia.
5. M. Adjoudj, M. Abid, A. Aissaoui, Y.. Ramdani, H. Bounoua, *Sliding Mode Control of a Doubly Fed Induction Generator for Wind Turbines*, Rev. Roum. Sci. Techn. – Electrotechn. Energ., **56,** *1*, pp. 15–24, 2011.
6. F. Belhachat, C. Larbes, L. Barazene, S. Kharz,. *Commande neuro-floue d'un hacheur MPPT*, 4th International Conference on Computer Integrated Manufacturing, 2007.

7. O. Gergaud, B. Multon, M. Ben Ahmed, *Analysis and experimental validation of various photovoltaic system model,*. 7th International Electrimacs Congres, Montreal, August 2002.
8. F. Z. Zerhouni, M. Kaddour Brahim, A. Boudghéne Stambouli, *Optimisation d'un système à énergie verte avec validation pratique*, Rev. Energie renouvelables, **11**, *1*, pp. 41–49, 2008.
9. R. Chibani, E.M. Berkouk, *Five-level PWM current rectifier-Five-level NPV VSI-Permanent magnet synchronous machine cascade*, The European Physical Journal – Applied Physics, **30**, pp. 135–148, 2005.
10. F. Bouchafaa, E.M. Berkouk, M.S. Boucheri, *Feedback control of DC link voltage of the BACK-TO-BACK PWM multilevel converter*, Journal of Electrical Engineering, **58**, *6*, pp. 318–325, 2007.
11. A. Aissaoui, M. Abid, H. Abid, A. Tahour, A. Zeblah, *A Fuzzy Logic Control for Synchronous Machine*, Journal of Electrical Engineering Elektrotechnicky Casopis (JEEEC), Bratislava, **58**, *5*, pp. 285–290, 2007.
12. A. Aissaoui, H. Abid, M. Abid,A.Tahour, *Fuzzy logic theory and sliding mode for a self-controlled sychronous machine*, Rev. Roum. Sci. Techn. – Electrotechn Energ, **52**, *1*, pp. 89–104, 2007.